Array Detection of a Moving Source

Javier Almendros[1], Bernard Chouet, and Phillip Dawson
U.S. Geological Survey

INTRODUCTION

Seismic arrays have been widely used for many years in aspects of seismology as diverse as the determination of the innermost structure of the Earth (Bataille *et al.*, 1990), the study of scattered waves to investigate the presence of heterogeneities in the crust (Gupta *et al.*, 1993), the verification of the Comprehensive Test Ban Treaty (Husebye and Mykkeltveit, 1981), the determination of rupture propagation velocity during earthquakes (Goldstein and Archuleta, 1991b), the determination of shallow velocity structures from analyses of sustained wave fields such as cultural noise (Aki, 1957; Horike, 1985) and volcanic tremor (Ferrazzini *et al.*, 1991; Métaxian *et al.*, 1997; Chouet *et al.*, 1998), and the location of volcanic sources (Almendros *et al.*, 2001b).

This versatility of seismic arrays is due to the fact that they sample the ground motion in both time and space, thus allowing a separation of the different wave components in the wavefield and providing an estimation of the instantaneous slowness vectors of these waves. This decomposition of the wavefield can be used to separate coherent wavefronts from noise, thereby improving the detectability of weak signals under noisy conditions. For this reason, seismic arrays are also referred to as "seismic antennas."

Information derived from the slowness vectors permits an estimation of the location of seismic sources, and in more general terms allows a spatiotemporal tracking of seismic sources. Tracking of the source is performed by monitoring the slowness vector parameters for any variation that may occur during the source activity. Most sources last a short time in comparison with the time required for the waves to travel from the source hypocenter to the receivers. For such sources, the slowness vectors obtained from array analyses performed on a moving window sliding across the seismograms of the event may be used to identify secondary phases such as scattered waves, but do not yield new information about the spatiotemporal properties of the source. Some seismic sources do last longer, however, and for these sources array tracking can, in theory and under certain conditions, provide enough information to determine the source trajectory or, if the source remains stationary, the source history.

To understand the difficulties involved in the spatial tracking of a seismic source, we may use the analogy of an airplane moving across the sky on a clear day. Under such conditions, one can point a finger to the plane's position and track its movement. In this familiar occurrence, there are a few unspoken concepts worth mentioning. First, we do not really know the plane's actual position. We know its direction, expressed perhaps as two angular coordinates, but we have no information on its distance to the observer. To determine the plane's exact location, one could use, for example, several observers spaced at distances comparable to that separating the plane from the ground and spread these observers over a wide range of azimuths surrounding the plane. In this situation, the crossing of the directions from each observer to the plane provides an estimate of the plane's position. Second, we are implicitly assuming that the speed of the plane is small compared with the velocity of light, so that the plane has not moved significantly during the time taken by light to reach us. But what if the sky is cloudy and we cannot see the plane but only hear it? The velocity of sound waves is comparable to the speed of the plane, so that we may not assume anymore that the plane is still in the direction our ears tell us the sound comes from. The plane was actually there some time earlier. How far the plane has moved from this position depends on the speed of the plane and its direction of motion relative to the observer. Third, we assume that the atmosphere is optically homogeneous, so that the ray paths are straight lines. But the presence of heterogeneities in the atmosphere further complicates the problem by introducing refraction, reflection, scattering, attenuation, and other wave-propagation phenomena. The light coming from the plane might not be monochromatic, opening the possibility of observing multiple images of different colors. Finally, the visual acuity of the observer plays a role too, in the sense that the image seen may not be a point of light but a blur instead.

Unfortunately, the seismological observation of a moving source in the Earth using multiple seismic antennas faces most of these problems. We can track the apparent slowness vectors of the wavefield and isolate the source components, but we do not know the distance to the source or the effects of the medium on the recorded signal. The source itself may be complex and generate waves with different kinds of polarizations, in preferred directions, and with frequency-dependent energy. The propagation medium contains three-dimensional heterogeneities in wave propagation velocity, density, rigidity, anelastic attenuation, and so on. To make matters worse, the seismological instrumentation filters our view of the wavefields via its limited bandwidth and dynamic

1. Now at Instituto Andaluz de Geofísica, Universidad de Granada, Spain.

range. The complexities involved are so daunting that, to our knowledge and apart from studies by Spudich and Cranswick (1984), Hough (1994), and Goldstein and Archuleta (1991b), who used a near-source array to track the rupture propagation along a fault during an earthquake, no spatial tracking of a moving seismic source has ever been attempted.

Estimating the distance to a source of any kind of sustained seismic signal is a challenging task, even for a stationary source. The lack of clear seismic phases and loss of coherence with distance make it impossible to locate accurately the sources of such signals with a traditional network. To address this problem small-aperture seismic antennas are required. Analyses of data from multiple synchronized antennas yield independent estimates of the slowness vectors of the wavefield. Each antenna provides a back-azimuth to the source, and an epicentral position can be determined from the intersections of all the back-azimuths. This simple geometrical method was applied by Almendros *et al.* (2000) to array data recorded at Teide Volcano (Canary Islands, Spain). Almendros *et al.* (2001a, b) later refined this method by including the effects of topography and 3D velocity structure on the wavefronts, and used the apparent slownesses of the waves to estimate the source depth. Another approach makes use of a circular wave-front assumption rather than the usual plane wave-front assumption. If the source is distant, there is no advantage in using this method. For nearby sources, however, the circular wave-front method can provide an estimate of the epicentral distance based on single-array data. Almendros *et al.* (1999) modified the array cross-correlation method of Del Pezzo *et al.* (1997) to account for receiver delays associated with circular wave fronts and obtained estimates of the epicenters of LP events in a swarm recorded by a single array at Deception Island Volcano, Antarctica.

In this article, we perform a detailed analysis of a sustained signal recorded simultaneously by two small-aperture seismic antennas deployed in Kilauea caldera, Hawaii. This signal is different from all other seismicity detected by the antennas. In order to understand its nature and behavior, we track the apparent slowness vectors recorded at both arrays to obtain an estimate of the source location. These analyses, combined with results from forward modeling, lead us to conclude that the detected signal corresponds to the signature of a moving source.

INSTRUMENTS

During the first weeks of February 1997, a seismic experiment was carried out at Kilauea Volcano, Hawaii, by a joint Japan-U.S. team. The purpose of this experiment was to identify active seismic sources within Kilauea. The deployed instruments include two small-aperture, semicircular seismic antennas named D and E (Figure 1), featuring Mark Products L11-4A and L22-3D sensors, each with a natural frequency of 2 Hz and sensitivity of 50 V/(m/s). Data were

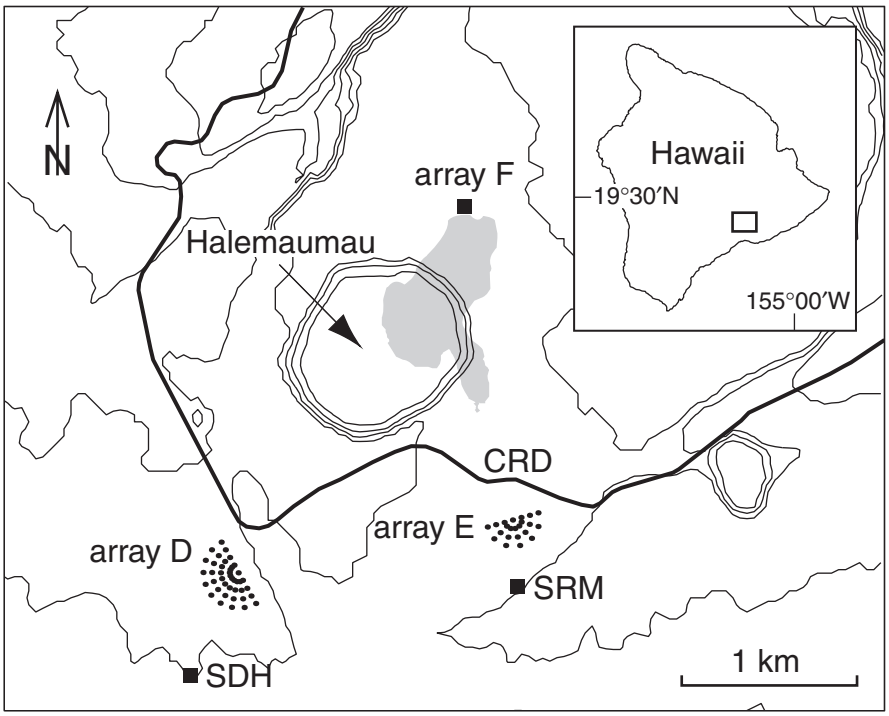

▲ **Figure 1.** Map of the southern sector of Kilauea caldera showing the positions and configurations of vertical sensors in the seismic antennas used in our analysis (black dots). The map contour interval is 25 m. The black squares mark the locations of two permanent stations of the Hawaiian broadband seismic network (SDH and SRM) and the center position of a third seismic antenna (F) not used in this study. The bold line shows Crater Rim Drive (CRD), a road that crosses the caldera south of the Halemaumau pit crater. The gray-shaded patch overlapping the eastern edge of Halemaumau represents the epicentral source region of the LP seismicity recorded during the experiment (Almendros *et al.*, 2001b). The inset shows the location of Kilauea caldera on the island of Hawaii.

sampled at 100 sps and recorded on 16-bit, three-channel Hakusan data loggers. Antenna D, with an aperture of 400 m, consists of 41 three-component sensors with station spacing of 50 m along the spokes and angular spacing of 20° between spokes. Antenna E, with an aperture of 300 m, includes 22 vertical-component sensors with station spacing of 50 m along the spokes and angular spacing of 30° between spokes.

DATA DESCRIPTION

In this section we describe different aspects of the signal recorded by antennas D and E between 13:20 and 13:30 (Hawaiian Standard Time) on 12 February 1997. The properties of this signal (waveform signature, spectral content, propagation direction, and apparent velocity) are unlike any other signal detected at Kilauea at the time. To understand the uniqueness of this signal, we compare it with the most common seismic signatures observed at Kilauea, those of long-period (LP) seismicity.

LP Seismicity

The term LP seismicity refers to a class of seismic events whose source processes involve interactions between fluids embedded in a solid medium, and the solid medium itself. The source mechanism of these events does not involve brittle shear failure, but rather the resonant excitation of fluid-filled cavities such as cracks or conduits (Chouet, 1988, 1992, 1996; Julian, 1994). The most important field where we encounter LP seismicity is volcano seismology. LP seismicity is fundamentally related to the dynamics of volcanoes and constitutes a very important tool in eruption forecasting (Chouet *et al.*, 1994; Chouet, 1996). Traditionally, LP seismicity includes two main types of events, LP events and tremor (Chouet, 1996). The distinction is based on the duration of activity, which is short for LP events (typically some tens of seconds, with longer coda reflecting a stronger impedance contrast between fluid and solid at the source) and longer for tremor (ranging up to several hours, or in some cases weeks or months). Other important characteristics such as spectral content, particle motions, and source location are usually the same for LP events and tremor (Fehler, 1983; Koyanagi *et al.*, 1987; Chouet *et al.*, 1994; Chouet, 1996; Almendros *et al.*, 1997; Almendros *et al.*, 2001b).

LP seismicity recorded at Kilauea during the February 1997 experiment was marked by a swarm of LP events superimposed on a sustained background of tremor. The peak in swarm activity occurred on 11 and 12 February, with almost one hundred LP events detected per hour. This LP seismicity was located by a method combining frequency-slowness analyses with the use of a slowness vector model (Almendros *et al.*, 2001a; Almendros *et al.*, 2001b). All hypocenters were found to be contained within a small volume of approximately 0.1 km^3 located at shallow depths northeast of the Halemaumau pit crater (Figure 1).

Waveform and Spectral Content

The most striking feature of the seismograms recorded between 13:20 and 13:30 on 12 February is the strong difference between the ground motions recorded at arrays D and E, located only 1.5 km apart. This is best demonstrated in the seismograms and spectrograms of 23 minutes of data obtained at two sample stations in arrays D and E (Figure 2). During this time interval, we observe several LP events (indicated by black arrows in Figure 2). LP events recorded at Kilauea are characterized by emergent onsets, spindle-shaped amplitude envelopes, and spectra containing energy in the band 1–15 Hz with dominant peaks in the 2–6 Hz range (Almendros *et al.*, 2001b). Individual event durations are typically about 20 s. These properties are common to the records from both antennas. However, between roughly 13:20 and 13:30 we find a portion of signal, marked by the white arrows in Figure 2, which appears quite different in both waveform and spectral content at arrays D and E. Most of the energy in this signal is concentrated in the band 7–20 Hz, except for the long-lasting presence of a spectral peak near 3 Hz. There is an apparent delay between the occurrence of this peak at array E and its occurrence at array D.

Propagation Properties

The propagation properties of a seismic signal are characterized in the plane wave-front approximation by the apparent slowness vector, **s**. The magnitude of this vector, called the ray parameter or apparent slowness, s, is the inverse of the apparent velocity of the wave fronts. Its direction represents the wave propagation azimuth, ϕ, usually measured clockwise from north. The apparent slowness and azimuth representing the apparent slowness vector can be estimated from frequency-slowness analyses of array data. In the present study, frequency-slowness analyses are performed using the MUSIC algorithm (Schmidt, 1986; Goldstein and Archuleta, 1987).

Our analyses are conducted over eleven overlapping frequency bands with individual bandwidths of 1.2 Hz, covering the overall bandwidth 1–10 Hz. The slowness spectra obtained in the different frequency bands are then stacked to obtain a more robust estimate of the slowness vector (Wang and Kaveh, 1985; Spudich and Oppenheimer, 1986). We use a window length of 2.56 s (256 samples) sliding in increments of 0.2 s across the records. Our analyses yield time series of slowness, azimuth, and power for each antenna, together with error limits in slowness and azimuth estimated from the dimensions of the slowness power contour corresponding to 90% of the maximum slowness power. Figure 3 shows two 90-second-long samples of frequency-slowness data from both antennas. These samples, recorded near the beginning and end of the period displayed in Figure 2, are dominated by LP seismicity. The occurrence of LP events and tremor is associated with the following observations: (1) There is a peak in the slowness power; (2) the azimuth remains stable for a few seconds with low error; (3) the slowness is generally low, indicating the presence of body waves; and (4) the features listed in (1), (2), and (3) are observed simultaneously at both anten-

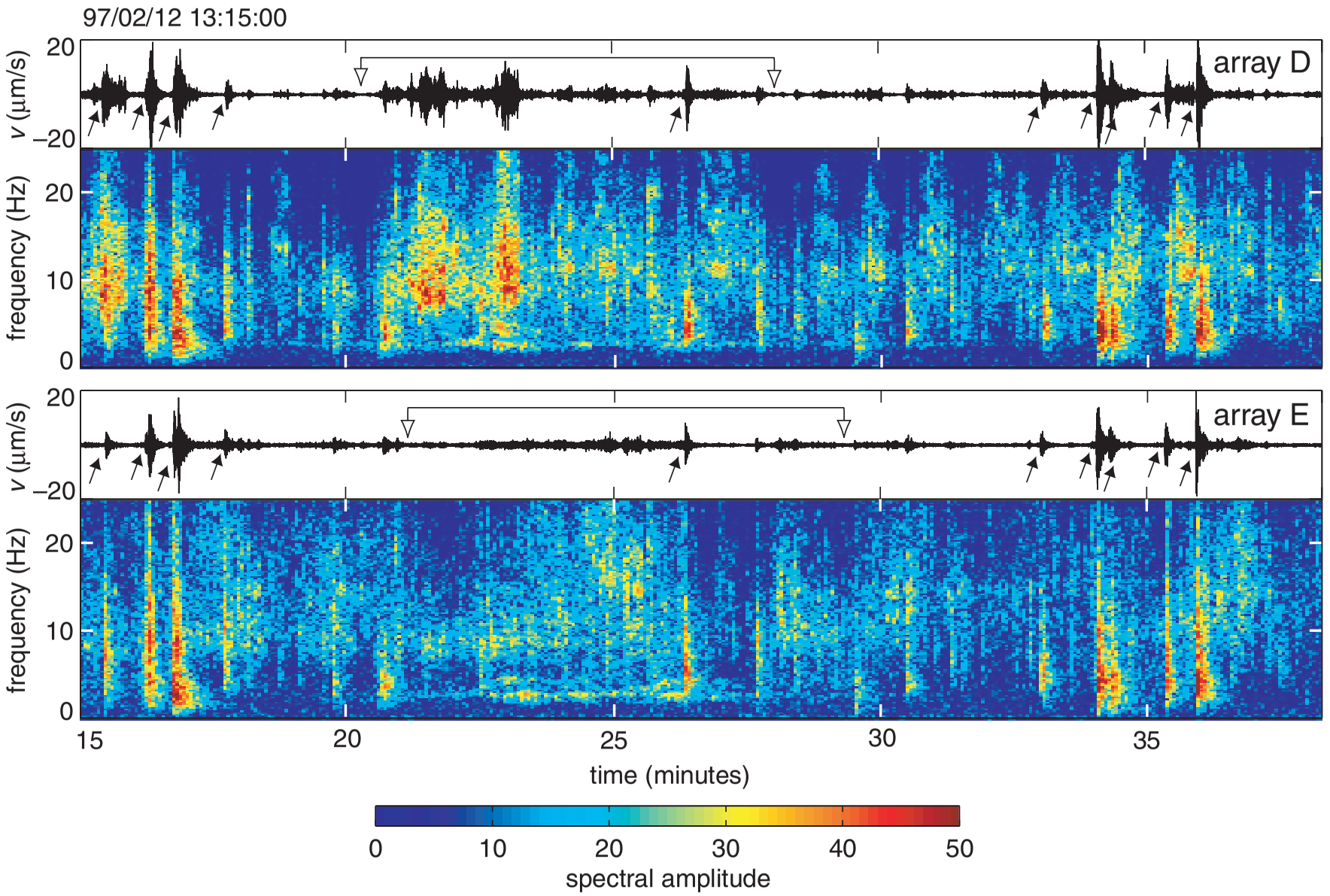

▲ **Figure 2.** Seismograms and spectrograms of data recorded at the hub stations in arrays D (top) and E (bottom) between 13:15 and 13:38 on 12 February 1997. The black arrows mark individual LP events, and the intervals bracketed by the white arrows mark the periods during which the sustained signal analyzed in the present study is most evident.

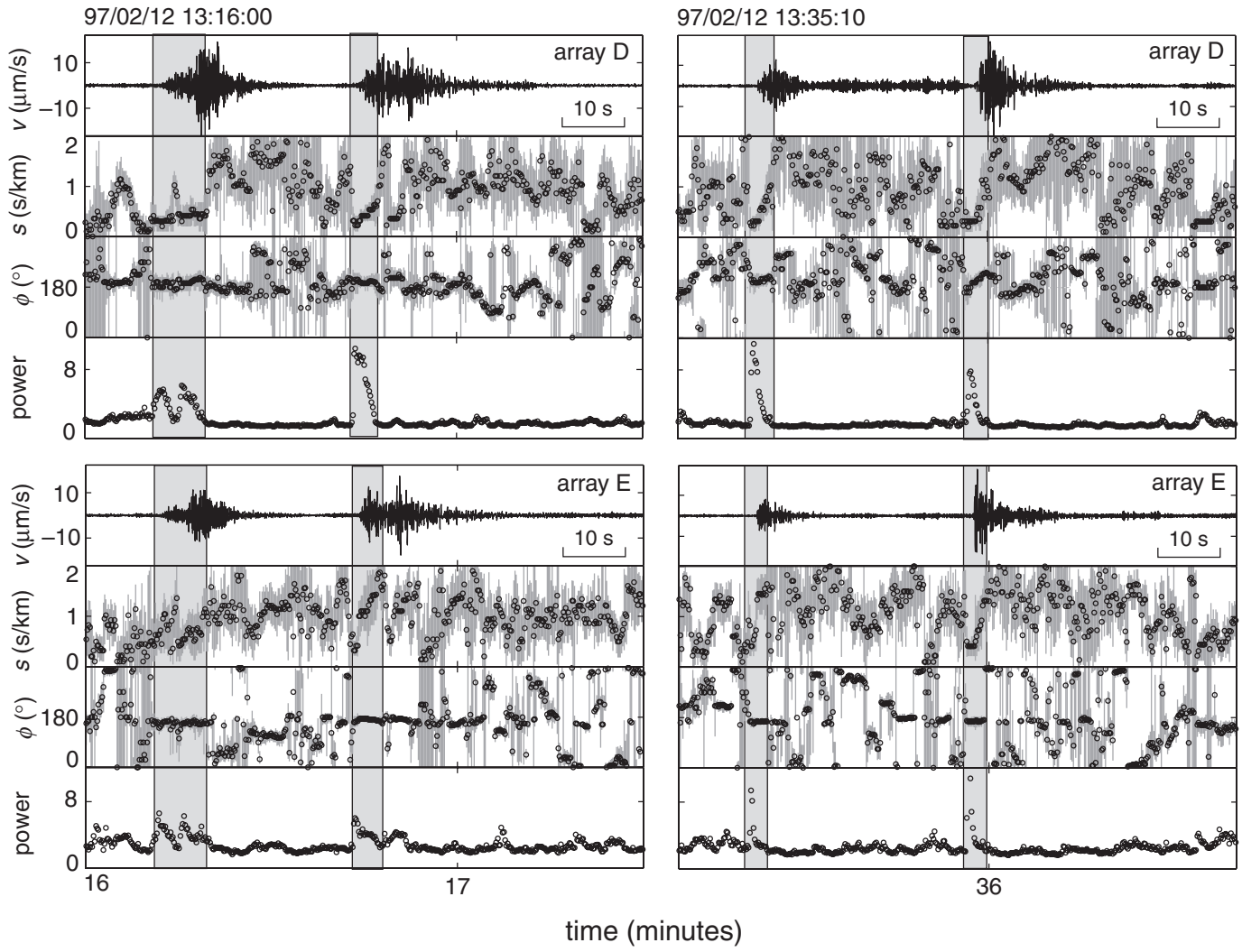

▲ **Figure 3.** Results of frequency-slowness analyses of LP seismicity performed on arrays D (top) and E (bottom) during the intervals 13:16:00–13:17:30 (left) and 13:35:10–13:36:40 (right) on 12 February 1997. The panels show, from top to bottom, the vertical component of ground velocity, *v*, recorded at the hub station, the apparent slowness, *s*, and azimuth, ϕ, together with their estimated errors and frequency-slowness power determined at each array. The vertical bands of shading bracket first arrivals for the LP events displayed.

nas. When LP events or tremor are not present in the wavefield, the slowness power remains low, and azimuth and slowness values are scattered and with large errors, indicating that the wavefield is dominated by noise.

Surprisingly, features quite distinct from those described above are observed in Figure 4, which shows frequency-slowness data for 6-minute-long records obtained at both arrays. These records contain the sustained signal occurring during the intervals bracketed by white arrows in Figure 2. Focusing on the portions of the signal highlighted by gray shading in Figure 4, we observe that (1) the slowness power fluctuates at a level slightly above background; (2) the azimuth displays small errors and remains almost stationary for several minutes, with a slow clockwise drift from an eastward to westward propagation; (3) the slowness is consistently high with values between 1 and 2 s/km, suggesting a wavefield dominated by surface waves, consistent with a shallow source; and (4) these features of the slowness data are not observed simultaneously at both antennas, but are first observed at antenna D and later at antenna E, with a delay on the order of one minute.

These two distinct behaviors are observed simultaneously in the frequency-slowness power spectra when the sustained signal and an LP event overlap. Waves generated by both sources contribute to the wavefield, with the dominant source producing the dominant spectral peak and the other source showing up as a secondary peak. As our analyses are focused in the main peak only, we detect one component or the other depending on their relative energy balance. Clear evidence of this effect is observed near the arrival time of the LP event at 13:26:20, marked by an arrow in Figure 4. Figure 5 shows the frequency-slowness results obtained for this section of data, which contains part of the sustained signal and an overlapping LP event. Before the LP event (during the

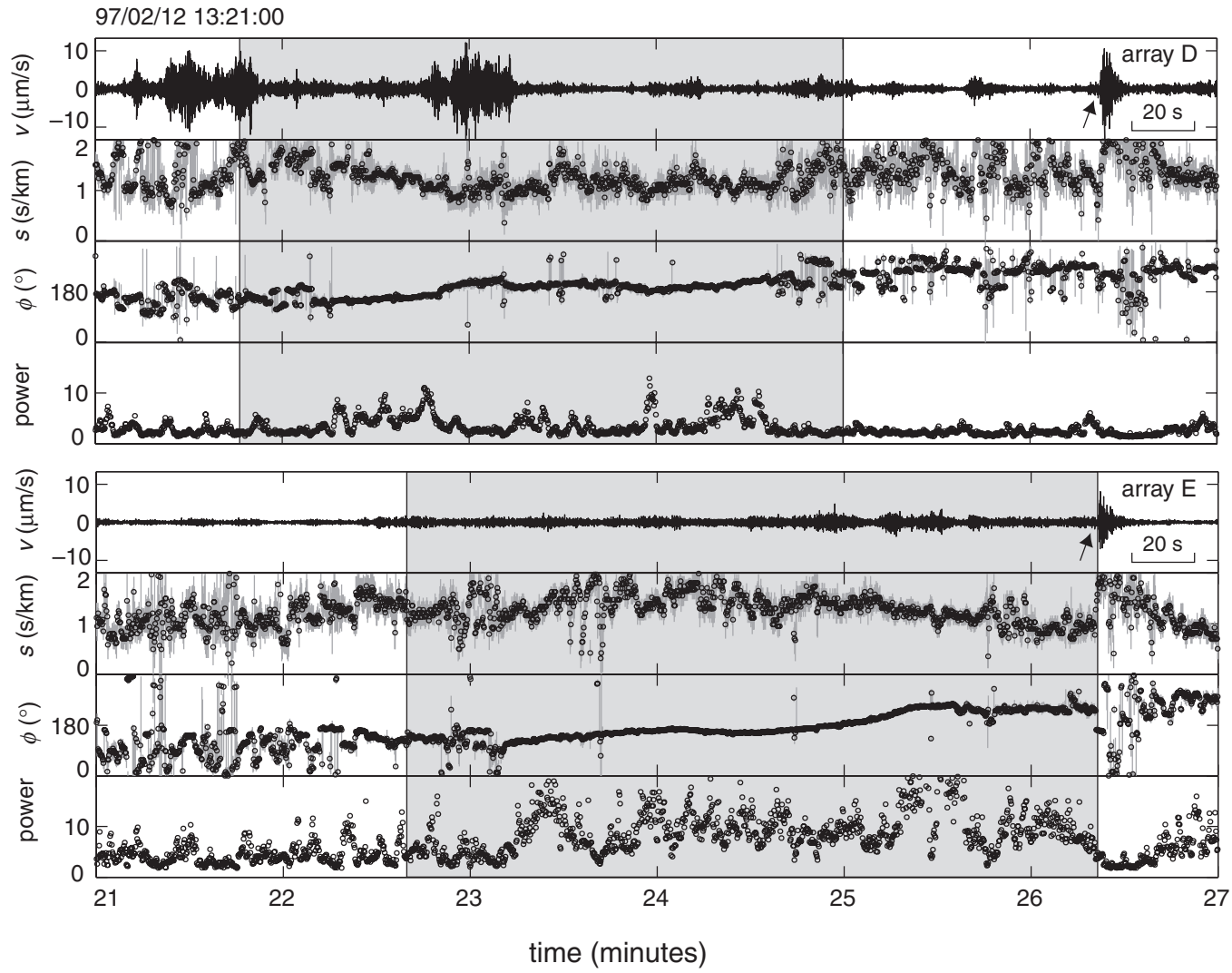

▲ **Figure 4.** Results of frequency-slowness analyses performed on arrays D (top) and E (bottom) for data corresponding to the sustained signal observed during the interval 13:21:00–13:27:00 on 12 February 1997. The panels show, from top to bottom, the vertical component of ground velocity, *v*, the apparent slowness, *s*, and azimuth, ϕ, together with their estimated errors and frequency-slowness power determined at each array. The shaded windows bracket the sustained signal analyzed in the present study. The black arrow marks an LP event superimposed on the sustained signal (see Figure 5).

period corresponding to the gray bands labeled "A"), the sustained signal is dominating the records and the azimuths are consistent with a source located east-northeast of both antennas. In contrast, at the onset of the LP event (the gray bands labeled "B") the source of the sustained signal becomes secondary and the azimuths point to another source located northeast of Halemaumau, coincident with the source of all the LP seismicity recorded during the experiment (Almendros *et al.*, 2001b).

ESTIMATION OF THE SOURCE LOCATION

We use two different methods to estimate the location of the source of the sustained signal shown in Figures 2 and 4. First, we obtain a geometrical location based only on azimuthal information from both antennas (Figure 6). The procedure consists in selecting an appropriate window at each antenna. Average values of azimuths and their errors are obtained at each antenna, and these estimates are used to locate the point where the two azimuthal directions intersect. A difficulty with this approach is that the windows selected at each antenna must contain the same wave fronts and thus should account for the delay in wave arrivals due to the spatial separation between the antennas. For LP events, this difficulty is resolved by looking at the coincidence of waveforms, power peaks, or similar wavefield features; however, for a sustained signal such as shown in Figure 4 there is no easy way to ensure that we are looking at the same wave arrivals at both antennas. Nevertheless, as our azimuthal data vary very slowly, we can obtain an approximate solution by using a window whose duration is longer than the largest expected delay between arrivals at each antenna. Accordingly, we select an 8-second-long window (Figure 6A) and restrict our analysis to the time interval 13:23:10–13:24:40, during which the frequency-slowness

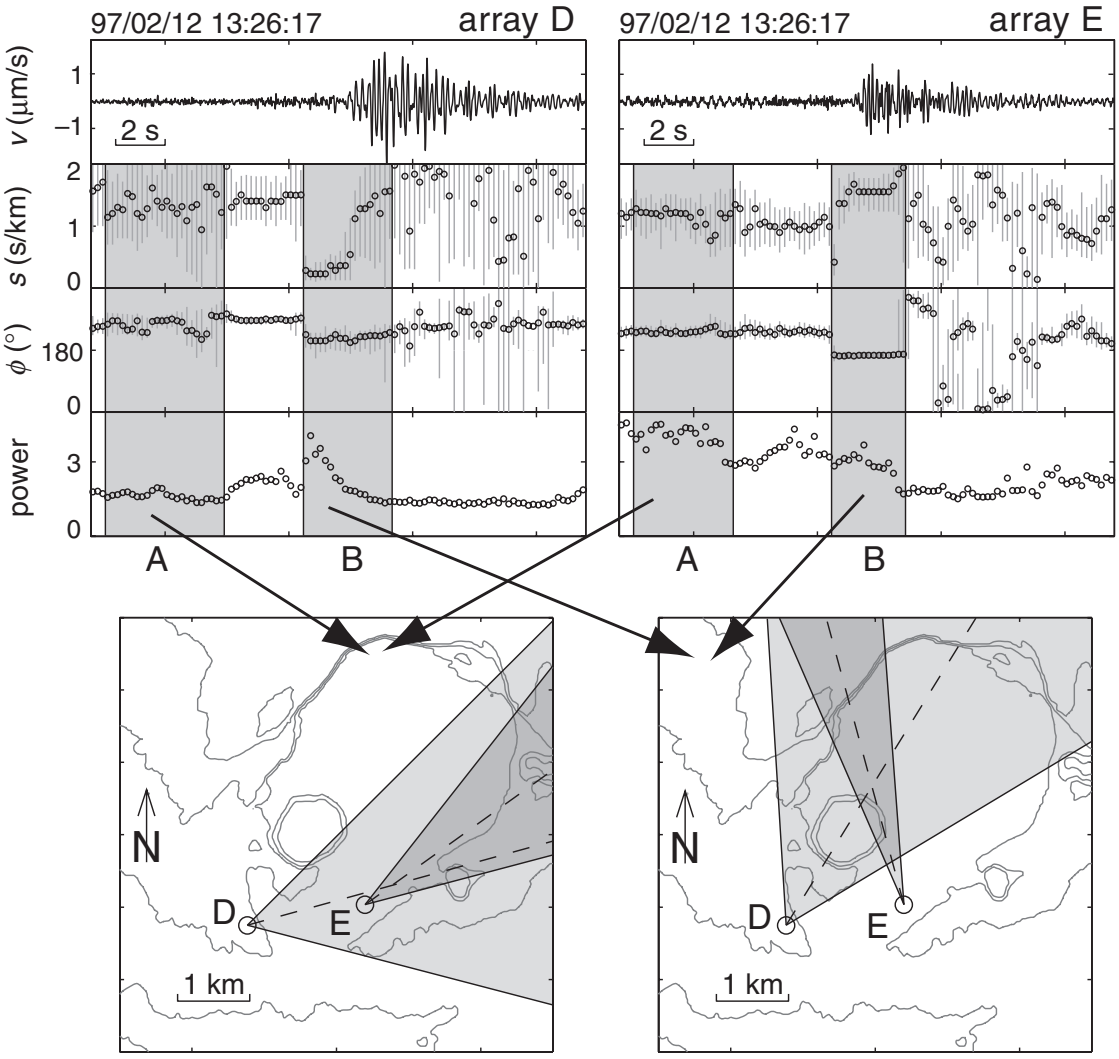

▲ **Figure 5.** Example of detection of an LP event superimposed on the sustained signal (see Figure 4). (top) Frequency-slowness results for arrays D (left) and E (right) for 20 s of data starting at 13:26:17 on 12 February 1997. The vertical bands of shading in the top panels identify parts of the wavefield dominated by the sustained signal (window A) and other parts of the wavefield dominated by first arrivals from an LP event (window B). (bottom) Trial locations obtained by averaging the values of azimuth within the shaded windows A and B in the top panels. The arrows indicate which windows were used in the solution. The dashed lines represent the average azimuths, and the shaded wedges represent the azimuthal spreads corresponding to the average errors in the azimuth estimates.

data from both arrays show slowly varying azimuths. By moving the window in increments of 0.4 s across this 90 s interval we obtain the apparent epicenters shown in Figure 6B.

Our second method is the circular wave-front method of Almendros *et al.* (1999). This method performs a cross-correlation of array data to obtain an estimation of the distance to the source. In our application of the method, we select a window length of 2.56 s and slide this window in increments of 0.2 s across the signal. We use only those results for which the difference in the maximum array-averaged cross-correlation (MACC) calculated for a circular wave front, compared to the MACC corresponding to a plane wave front, exceeds a certain threshold value, fixed to 5% of the plane wave-front MACC. An application of this method to our data reveals that during most of the selected time interval the source is too far to allow an accurate estimation of its distance to our antennas. Only two time intervals are found—one for each antenna—during which the circular wave-front method provides meaningful estimates of the epicentral distance to the source. Figure 7 shows the distance estimates obtained between 13:20 and 13:28. Solutions with less than 5% of MACC improvement are represented by crosses, and those with MACC improvement larger than 5% are shown by dots. In these plots, we observe that the source was close to each antenna during a short period of time. The source is near antenna D during the time interval 13:22:40–13:23:40 and is near antenna E during the interval 13:24:10–13:25:20. The durations of the intervals of source proximity to each antenna are both about one minute, and the delay between each interval is on the order of 100 s.

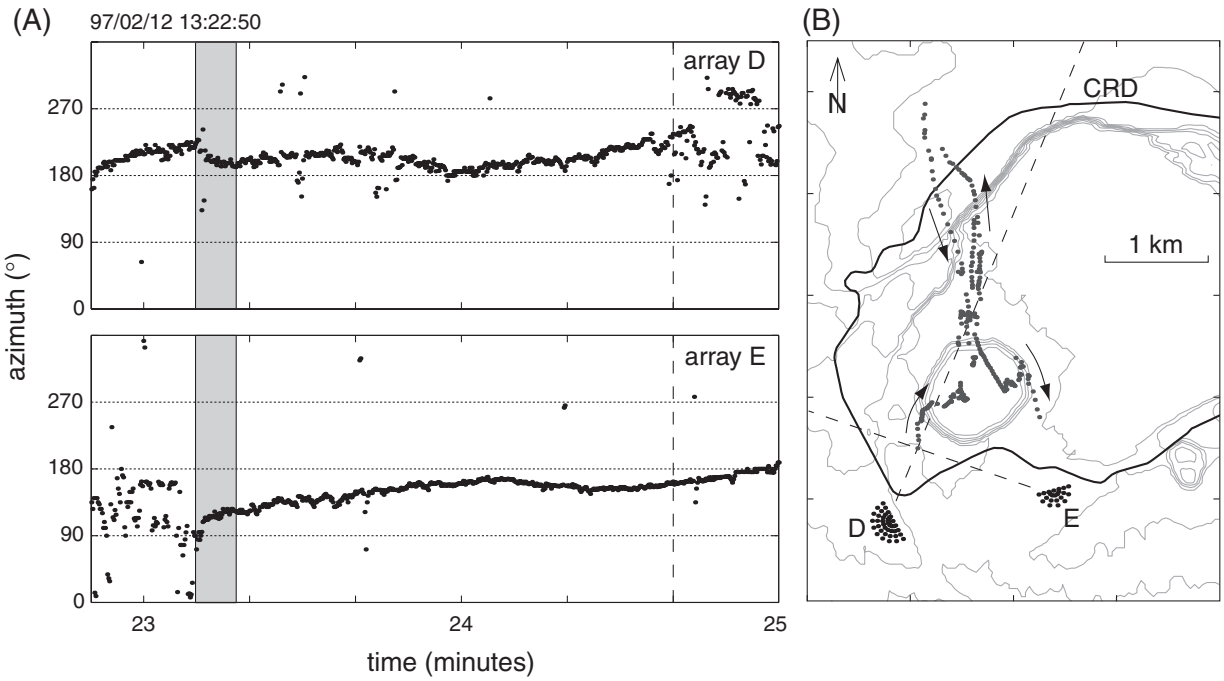

▲ **Figure 6.** (A) Azimuths obtained from frequency-slowness analyses of data from arrays D (top) and E (bottom) for 130 s of record starting at 13:22:50 on 12 February 1997. The shaded interval identifies an 8-second-long window. This sliding window steps in increments of 0.4 s across the records from both antennas, starting at the displayed position and ending at a time marked by the dashed vertical line. The overall time interval considered extends from 13:23:10 to 13:24:40, during which both antennas are detecting a stable wave-propagation azimuth. An average back-azimuth is calculated for each window at each antenna to obtain an estimate of the source epicenter from the intersection of the two back-azimuths. (B) Apparent trajectory of the source epicenter obtained by this location method. The two dashed lines show the average back-azimuths at antennas D and E at the time corresponding to the center position of the shaded window in (A). Dots mark epicenter positions obtained in successive time windows, and arrows indicate the directions of apparent source motion.

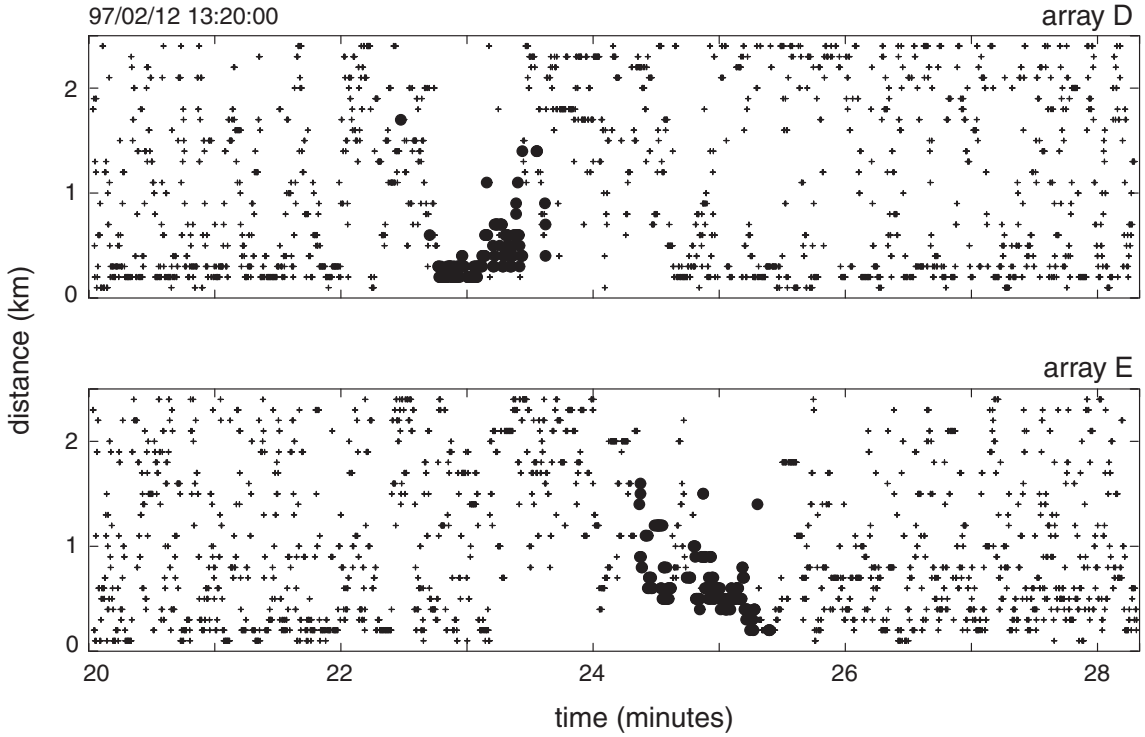

▲ **Figure 7.** Distance to the source estimated by the circular wave-front method. Low confidence results are marked by small crosses, and reliable results are shown as solid dots.

DISCUSSION

Origin of the Signal

The first hint that emerges from the results of our analyses is that we are dealing with a sustained source, in the sense that the character of the waves remains approximately the same during the entire time interval highlighted by the gray windows in Figure 4. If discrete sources were present, we would observe the characteristics of the noise between source bursts, but we see no evidence of that. Being on a volcano, we might naturally think that the origin of the sustained signal could be a low-amplitude volcanic tremor, with the differences in the traces observed at both arrays being due to path or site effects. Sustained tremor has been observed at many volcanoes and is usually associated with continuous degassing, venting, and other processes of fluid transport (Fehler, 1983; Chouet, 1996). However, taking into account the odd characteristics of the signal observed at 13:20 as compared to LP seismicity, we cannot think of any natural process that might be responsible for its origin. The observed temporal variation in the propagation azimuths can be satisfactorily explained only if the source is actually moving. The azimuthal variation of up to 2°/s translates into a transverse velocity of 17 m/s (or 61 km/h) at a distance of 500 m from the antenna, and 70 m/s (251 km/h) at a distance of 2 km. This is manifestly too fast for the propagation of a dike or any other natural source. The propagation of the rupture along a long earthquake fault is also excluded because the antennas are very close compared to the fault length, so that they should detect waves with similar azimuths, which is not the case. Furthermore, the signal is not simultaneously detected at arrays D and E even when we account for a reasonable delay due to wave propagation. Surface-wave velocities in this volcanic environment may be in the range 0.6–0.8 km/s for 3 Hz waves (Ferrazzini *et al.*, 1991), so that for the distance of roughly 1.5 km separating the two antennas the maximum expected signal delay between antennas is 1.8–2.5 s. We find that the signal is delayed by over one minute at antenna E compared to antenna D, hence this delay cannot be related to wave propagation, and we conclude that it reflects the motion of the source.

Our interpretation of these observations is that a nonnatural seismic source is moving across Kilauea caldera. This source generates a low-energy signal that is detected only when the source is close enough to the antennas. Our immediate assumption for such a source is a heavy vehicle moving eastward along Crater Rim Drive (CRD), a road surrounding Kilauea caldera (Figure 1). This road traverses the caldera just south of Halemaumau and passes within a few hundred meters of both antennas. For a vehicle moving counterclockwise from north to east along the road (Figure 1), the wave propagation azimuth should shift from eastward to westward in a clockwise rotation, as observed. The apparent slowness should be high, corresponding to a source at the surface of a medium consisting of low-impedance surficial volcanic deposits, again in qualitative agreement with what we observe in our data. Our estimation of distance to the source based on the circular wave-front method is also consistent with the vehicle hypothesis. Results from this analysis show that the source is within a few hundred meters of each antenna during at least 60 s and that it takes about 100 s to move from the vicinity of antenna D to the vicinity of antenna E. Along the road, the distance between both antennas is about 1.7 km. This distance can be traveled in 100 s by a vehicle moving at 60 km/h. Therefore, the vehicle hypothesis qualitatively explains many characteristics of the observed data.

Additional evidence favoring the vehicle hypothesis comes from other instruments deployed during the 1997 experiment, and in particular from a third seismic antenna located immediately northeast of Halemaumau (array F in Figure 1). Frequency-slowness analyses performed on data recorded on this antenna did not show any trace of the sustained signal observed at antennas D and E. As a vehicle moving along the CRD never gets closer than 1.5 km to this third antenna, the source is always too distant and the signal-to-noise ratio too low to allow its detection at this location.

Further support for our vehicle hypothesis is two examples of vehicle traces shown in Figure 8. These traces were recorded at stations SDH and SRM of the Hawaiian broadband seismic network (see Figure 1) at other times than the period analyzed here. Station SDH is located near array D, and both the station and array are located on the same sandy hill. Station SRM is near array E, and in this case both the station and array are on the same pahoehoe flow. The records obtained at both stations show a behavior similar to the signal we have analyzed and display completely different features at the two stations. An energetic high-frequency wave train is observed at SDH, which is not seen at SRM. Signals with similar features are most commonly observed in the records of SDH and SRM during daytime hours. Such signals are interpreted by the HVO staff as signatures of vehicles moving along the CRD.

There is, however, an inconsistency between the above conceptual model of the source and our estimation of distance derived from the joint location method. As shown in Figure 6B, during the time interval when the source is between the two antennas, the source appears to move north, away from CRD, very fast, drifting by 4 km in about 30 s at an average velocity of 480 km/h. This is too fast for any vehicle, even considering a helicopter moving close to the ground. We note, however, that this peculiar source trajectory appears to overlap with the topographic features associated with the circular edge of the Halemaumau pit crater. A possible explanation for the observed trajectory may thus be that the energy contributions to the wavefield from secondary reflections and diffractions by the topography of Halemaumau are stronger than the energy contributions from the primary source moving along CRD. The trajectory shown in Figure 6B would then be only an apparent trajectory resulting from the fact that the antennas are pointing to the edges of Halemaumau instead of the actual source position. The short wavelengths of the waves make them particularly sensitive to small-scale topographic features of the volcanic medium.

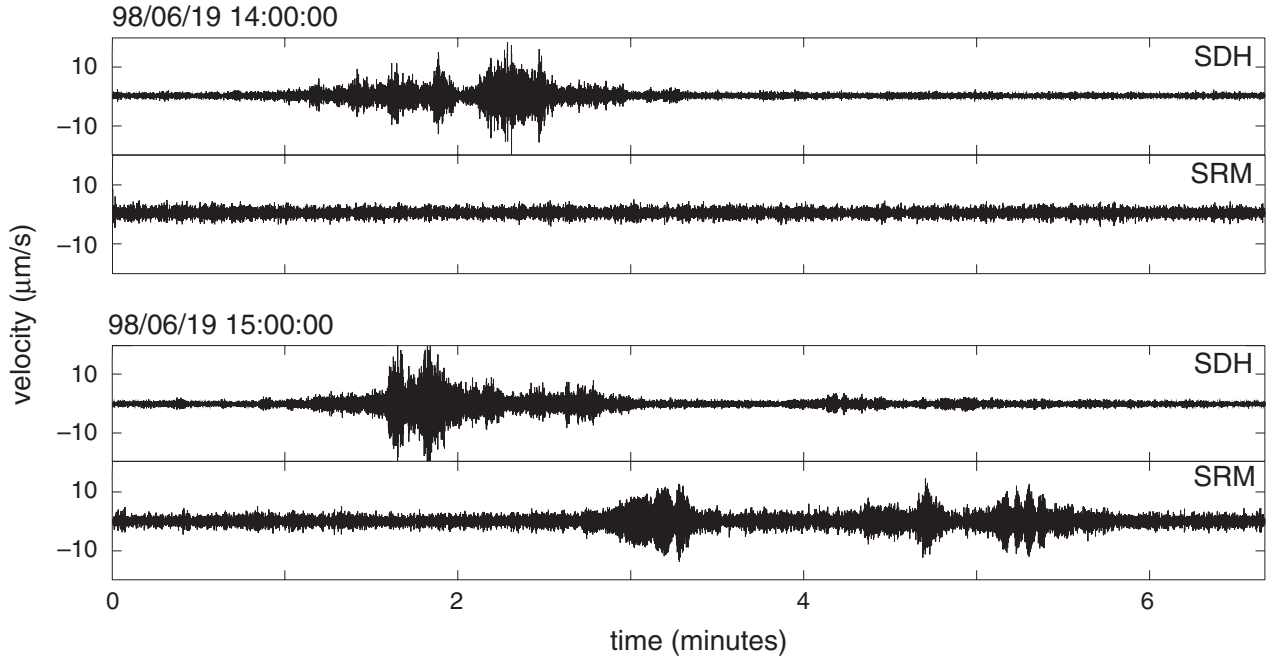

▲ **Figure 8.** Examples of two signals recorded at stations SDH and SRM (see Figure 1) with features similar to those of the sustained signal analyzed in the present paper (compare to seismograms in Figure 2). Station SDH is located near array D, and station SRM is located near array E.

Modeling a Source Moving along the CRD

As a final step, we test our hypothesis by attempting to model the azimuths that the antennas should detect for a vehicle moving along CRD. The simple model we develop here assumes that the medium is homogeneous. In such a medium the propagation azimuths of the waves observed at the antennas represent the geometrical azimuths from the source to the center of each antenna. Our goal is to compare the azimuths associated with given positions along CRD with the propagation azimuths derived from our array analyses. To perform this comparison, we assume an instantaneous velocity for the vehicle based on our experience of driving along CRD and a fixed apparent slowness s = 1.5 s/km.

We divide CRD into N segments of length l_n (n = 1, 2, … , N), starting at an arbitrary origin position, and assume a fixed vehicle velocity v_n in each segment. The time spent by the vehicle in segment n is $\tau_n = l_n/v_n$. Denoting the coordinates of the end of the nth segment and antenna center by (x_n, y_n) and (x_0, y_0), respectively, we obtain the propagation azimuth ϕ_n and distance to the antenna r_n as the source passes that segment, in the forms

$$\phi_n = \tan^{-1}\frac{x_0 - x_n}{y_0 - y_n}$$
$$r_n = \sqrt{(x_0 - x_n)^2 + (y_0 - y_n)^2}. \qquad (1)$$

The arrival time t_n of the waves at the antenna is the sum of the time spent by the waves to propagate from the source to the antenna, plus the time spent by the source to propagate from the first to the nth segment of the road,

$$t_n = s \cdot r_n + \sum_{i=1}^{n} \tau_i \,. \qquad (2)$$

In this manner, we obtain a series (t_n, ϕ_n) that can be compared with the experimental azimuthal data. To overlay the experimental and synthetic azimuth traces we need to synchronize them. The origin time depends on our selection of an origin along the road, and the corresponding time delay must be adjusted manually.

Using this procedure we obtain the results shown by solid lines in Figure 9. Our fit reproduces the overall behavior of the data, although several details are not explained, such as the secondary maximum on array E at 13:24:10 and the consistently lower azimuth at D during the interval 13:23:50–13:24:30. This may be an indication that our assumptions concerning the medium are not correct, and that topography and velocity heterogeneities play an important role in the wave propagation.

Further refinement can be achieved by including the effect of topography on the propagating wavefronts. Using the Kilauea topography, we perform finite difference calculations (Ohminato and Chouet, 1997) for a point source moving along CRD. These calculations consider a domain of $8 \times 8 \times 2$ km discretized by $401 \times 401 \times 101$ cells with fixed size of $20 \times 20 \times 20$ m. The top layer of cells is centered at the geographical coordinates 19′24.5°N, 155′17.0°W, at an elevation of 1,277 m. Lamé coefficients are set to zero in all the cells located above the topography. Our simulation considers successive sources distributed along the discretized track of CRD. As before, CRD is divided into N segments of

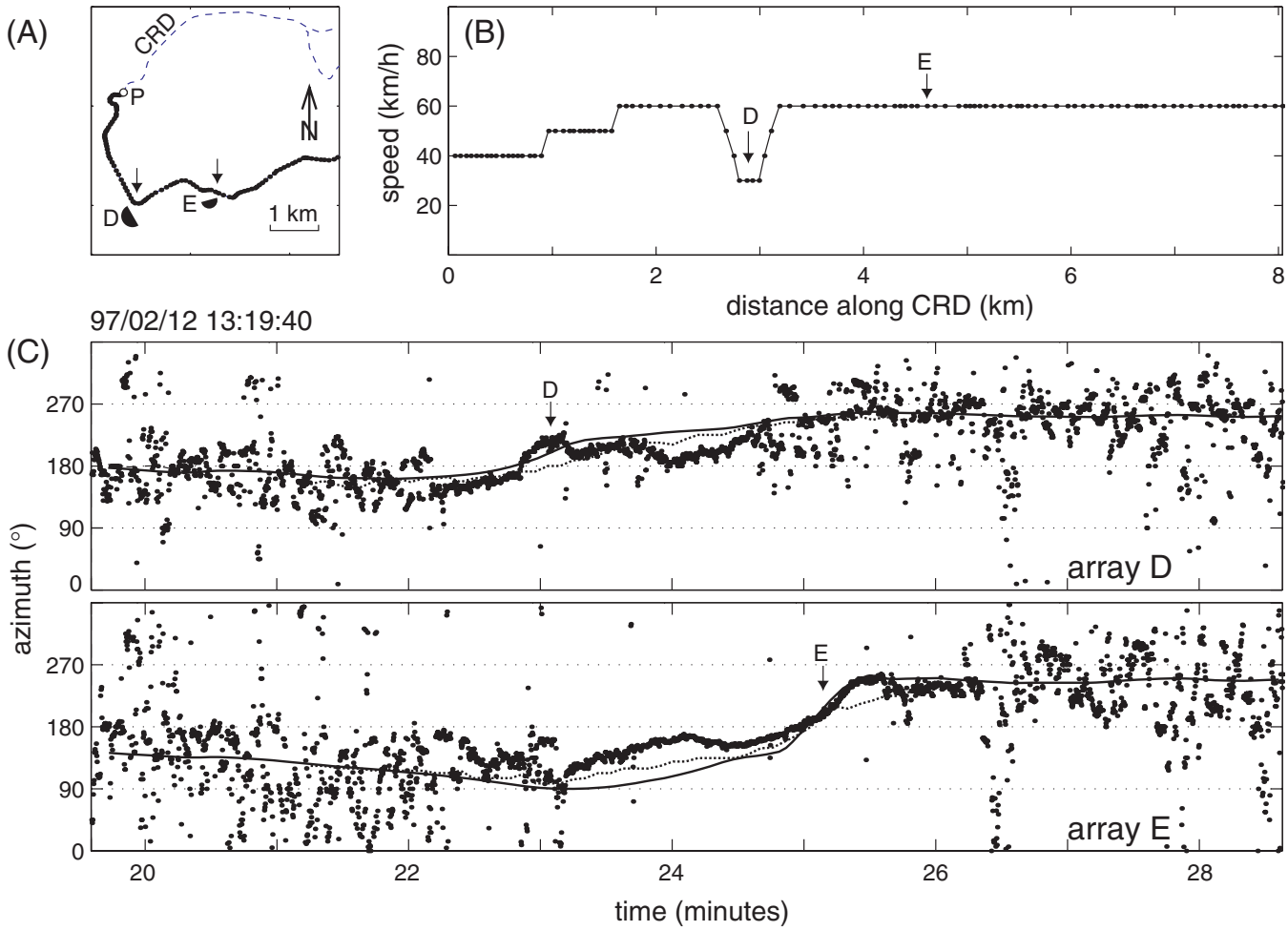

▲ **Figure 9.** Forward modeling of the wave-propagation azimuths detected by the two antennas. Our model is based on the geometrical directions from the road to the center of each array and an assumed velocity history of the source. (A) Map view of the location of the antennas relative to CRD. Black dots mark the ends of the road segments considered in our calculation. The origin used for the measurement of distances along the road is marked by an open circle labeled P. (B) Vehicle velocity as a function of distance from the origin P. (C) Wave-propagation azimuths obtained from frequency-slowness analyses of the data (solid dots), azimuths calculated with the geometric model (solid line), and azimuths obtained from finite-difference calculations (dotted line) for arrays D (upper panel) and E (bottom panel). The arrows in (A), (B), and (C) mark the road locations closest to each antenna.

length l_n and one source is applied at the center of each segment. The origin time of each source is fixed by the velocity profile shown in Figure 9B. Each source consists of a single downward vertical force with amplitude of 10^5 N, and source-time function $S(t)$ in the form of an exponentially decaying sine function

$$S(t) = t^m \exp(-t/\tau) \sin(2\pi f t) \qquad (3)$$

where $m = 4$, $\tau = 0.2$ s, and $f = 3$ Hz. The total duration of a source is ~2 s, so that the signal from each source overlaps with the signal from the next triggered source, thereby producing a sustained signal. The synthetic wavefield generated in this manner is analyzed with synthetic antennas that simulate the locations and configurations of antennas D and E. Frequency-slowness analyses of the synthetic wavefield, performed using the same parameters as those applied to the actual data, yield time series of azimuths that can be compared with the experimental data.

The results of this procedure are shown by the dotted lines in Figure 9. The synthetic azimuthal curves obtained by finite difference are generally closer to the experimental data than those based on the simple geometrical model (solid lines), corroborating our assumption concerning the importance of topography effects in the wavefield. However, details of the azimuthal behavior of the data are still not fully explained. The next obvious step in modeling these data would be to include information about the three-dimensional velocity structure. Unfortunately, our knowledge of small-scale velocity heterogeneities in the Kilauea summit region is still too incomplete to attempt resolving these details. In particular, the 3D velocity model of Kilauea caldera with resolution of 500 m obtained by Dawson *et al.* (1999) is too smooth to allow a better fit to our azimuthal data.

CONCLUSIONS

The present analysis provides a demonstration of the capabilities of small-aperture seismic antennas. We have used frequency-slowness analyses to track the apparent slowness vectors of the wavefield, and two distance-estimation methods in attempts to convert this information into a spatial tracking of the epicenter. Although we are fairly confident that the sustained signal represents the seismic signature of a vehicle traveling along CRD, we cannot model this source in detail because of simplifying assumptions required by our limited knowledge of the fine-scale velocity structure of the medium.

ACKNOWLEDGMENTS

We thank Chris Huber, who first discovered the sustained signal analyzed in this paper. We are also grateful to Y. Ida, T. Iwasaki, N. Gyoda, J. Oikawa, M. Ichihara, Y. Goto, T. Kurihara, M. Udagawa, and K. Yamamoto of the Earthquake Research Institute, University of Tokyo; K. Yamaoka, M. Nishihara, and T. Okuda of Nagoya University; H. Shimizu and H. Yakiwara of Kyushu University; E. Fujita of the National Research Institute for Earth Science and Disaster Prevention, Tsukuba; T. Ohminato of the Geological Survey of Japan, Tsukuba; S. Adachi of Hakusan Corporation; C. Dietel and P. Chouet of the U.S. Geological Survey, Menlo Park; P. Okubo, A. Okamura, M. Lisowski, M. Sako, K. Honma, and W. Tanigawa of the U.S. Geological Survey, Hawaiian Volcano Observatory; S. McNutt, D. Christensen, and J. Benoit of the University of Alaska, Fairbanks; and S. Kedar of the California Institute of Technology, Pasadena for their participation in the field experiment. In particular we wish to thank Y. Ida, whose exceptional organizational skills made this experiment possible. Funding for the experiment was provided by a grant from the Japanese Ministry of Education (Monbusho) to the Earthquake Research Institute of the University of Tokyo. David Oppenheimer, Paul Spudich, and Susan Hough contributed with constructive comments. The work by J. Almendros was partially supported by a fellowship from the Spanish Ministry of Education and by projects ANT-1111, REN-2000-2897, and REN-2001-3833 of the Spanish Ministry of Science and Technology.

REFERENCES

Aki, K. (1957). Space and time spectra of stationary stochastic waves, with special reference to microtremors, *Bull. Earthq. Res. Inst. Tokyo Univ.* **25**, 415–457.

Almendros, J., J. Ibáñez, G. Alguacil, E. Del Pezzo, and R. Ortiz (1997). Array tracking of the volcanic tremor source at Deception Island, Antarctica, *Geophys. Res. Lett.* **24**, 3,069–3,072.

Almendros, J., J. Ibáñez, G. Alguacil, and E. Del Pezzo (1999). Array analysis using circular wavefront geometry: An application to locate the nearby seismo-volcanic source, *Geophys. J. Int.* **136**, 159–170.

Almendros, J., B. Chouet, and P. Dawson (2001a). Spatial extent of a hydrothermal system at Kilauea Volcano, Hawaii, determined from array analyses of shallow long-period seismicity, 1. Method, *J. Geophys. Res.* **106**, 13,565–13,580.

Almendros, J., B. Chouet, and P. Dawson (2001b). Spatial extent of a hydrothermal system at Kilauea Volcano, Hawaii, determined from array analyses of shallow long-period seismicity, 2. Results, *J. Geophys. Res.* **106**, 13,581–13,597.

Almendros, J., J. Ibáñez, G. Alguacil, J. Morales, E. Del Pezzo, M. La Rocca, R. Ortiz, V. Araña, and M. J. Blanco (2000). A double seismic antenna experiment at Teide Volcano: Existence of local seismicity and lack of evidences of volcanic tremor, *J. Volcan. Geotherm. Res.* **103**, 439–462.

Bataille, K., R. Wu, and S. Flatté (1990). Inhomogeneities near the core-mantle boundary evidenced from scattered waves: A review, *Pageoph* **132**, 151–173.

Chouet, B. (1988). Resonance of a fluid-driven crack: Radiation properties and implications for the source of long-period events and harmonic tremor, *J. Geophys. Res.* **93**, 4,375–4,400.

Chouet, B. (1992). A seismic model for the source of long-period events and harmonic tremor, in R. W. Johnson, G. Mahood, and R. Scarpa (editors), IAVCEI *Proceedings in Volcanology*, Vol. 3, Springer-Verlag, Berlin, 133–156.

Chouet, B. (1996). Long-period volcano seismicity: Its source and use in eruption forecasting, *Nature* **380**, 309–316.

Chouet, B., R. A. Page, C. D. Stephens, J. C. Lahr, and J. A. Power (1994). Precursory swarms of long-period events at Redoubt Volcano (1989–1990), Alaska: Their origin and use as a forecasting tool, *J. Volcan. Geotherm. Res.* **62**, 95–135.

Chouet, B., G. Saccorotti, M. Martini, P. Dawson, G. De Luca, G. Milana, and R. Scarpa (1997). Source and path effects in the wave fields of tremor and explosions at Stromboli volcano, Italy, *J. Geophys. Res.* **102**, 15,129–15,150.

Chouet, B., G. De Luca, G. Milana, P. Dawson, M. Martini, and R. Scarpa (1998). Shallow velocity structure of Stromboli volcano, Italy, derived from small-aperture array measurements of strombolian tremor, *Bull. Seism. Soc. Am.* **88**, 653–666.

Dawson, P., B. Chouet, P. Okubo, A. Villaseñor, and H. Benz (1999). Three-dimensional velocity structure of the Kilauea caldera, Hawaii, *Geophys. Res. Lett.* **26**, 2,805–2,808.

Del Pezzo, E., J. Ibáñez, and M. La Rocca (1997). Observations of high-frequency scattered waves using dense arrays at Teide volcano, *Bull. Seism. Soc. Am.* **87**, 1,637–1,647.

Fehler, M. (1983). Observations of volcanic tremor at Mount St. Helens volcano, *J. Geophys. Res.* **88**, 3,476–3,484.

Ferrazzini, V., K. Aki, and B. Chouet (1991). Characteristics of seismic waves composing Hawaiian volcanic tremor and gas-piston events observed by a near-source array, *J. Geophys. Res.* **96**, 6,199–6,209.

Goldstein, P. and Archuleta (1987). Array analysis of seismic signals, *Geophys. Res. Lett.* **14**, 13–16.

Goldstein, P. and R. Archuleta (1991a). Deterministic frequency-wavenumber methods and direct measurements of rupture propagation during earthquakes using a dense array: Theory and methods, *J. Geophys. Res.* **96**, 6,173–6,185.

Goldstein, P. and R. Archuleta (1991b)., Deterministic frequency-wavenumber methods and direct measurements of rupture propagation during earthquakes using a dense array: Data analysis, *J. Geophys. Res.* **96**, 6,187–6,198.

Goldstein, P. and B. Chouet (1994). Array measurements and modeling of sources of shallow volcanic tremor at Kilauea volcano, Hawaii, *J. Geophys. Res.* **99**, 2,637–2,652.

Gupta, I. N., C. S. Lynnes, T. W. McElfresh, and R. A. Wagner (1990). F-k analysis of NORESS array and single station data to identify sources of near-receiver and near-source scattering, *Bull. Seism. Soc. Am.* **80**, 2,227–2,241.

Gupta, I. N., C. S. Lynnes, and R. A. Wagner (1993). An array study of the effects of a known local scatterer on regional phases, *Bull. Seism. Soc. Am.* **83**, 53–63.

Horike, M. (1985). Inversion of phase velocity of long-period microtremors to the S wave velocity structure down to the basement in urbanized areas, *J. Phys. Earth* **33**, 59–96.

Hough, S. E. (1994). Southern surface rupture associated with the M 7.3 Landers, California, earthquake, *Bull. Seism. Soc. Am.* **84**, 817–825.

Husebye, E. and S. Mykkeltveit (editors) (1981). Identification of seismic sources: Earthquakes or underground explosions, Proc. NATO Advanced Study Institute Series, D. Reidel Publishing Co., Dordrecht.

Julian, B., D. Davies, and R. Sheppard (1972). PKJKP, *Nature* **235**, 317–318.

Julian, B. R. (1994). Volcanic tremor: Nonlinear excitation by fluid flow, *J. Geophys. Res.* **99**, 11,859–11,877.

Koyanagi, R. Y., B. Chouet, and K. Aki (1987). Origin of volcanic tremor in Hawaii, part I, in R. W. Decker, T. L. Wright, and P. H. Stauffer (editors), *Volcanism in Hawaii*, USGS Prof. Paper 1350, 1,221–1,257.

Métaxian, J.-P., P. Lesage, and J. Dorel (1997). Permanent tremor at Masaya Volcano, Nicaragua: Wave field analysis and source location, *J. Geophys. Res.* **102**, 22,529–22,545.

Ohminato, T. and B. Chouet (1997). A free-surface boundary condition for including 3D topography in the finite-difference method, *Bull. Seism. Soc. Am.* **87**, 494–515.

Schmidt, R. O. (1986). Multiple emitter location and signal parameter estimation, *IEEE Trans. Ant. Prop.* **34**, 276–280.

Spudich, P. and E. Cranswick (1984). Direct observation of rupture propagation during the 1979 Imperial Valley earthquake using a short baseline accelerometer array, *Bull. Seism. Soc. Am.* **74**, 2,083–2,114.

Spudich, P. and D. Oppenheimer (1986). Dense seismograph array observations of earthquake rupture dynamics, in S. Das, J. Boatwright, and C. Scholz (editors), *Earthquake Source Mechanism*, Geophys. Monogr. Ser. 37, AGU, Washington, 285–296.

Tono, Y. and K. Yomogida (1996). Complex scattering at the core-mantle boundary observed in short-period diffracted P-waves, *J. Phys. Earth* **44**, 729–744.

Wang, H. and M. Kaveh (1985). Coherent signal-subspace processing for the detection and estimation of angles of arrival of multiple wide-band source, *IEEE Trans. Acoust. Speech Signal Proc.* **33**, 823–831.

Instituto Andaluz de Geofísica
Universidad de Granada
Campus de Cartuja
18071 Granada
Spain
telephone: +34-958-249552
fax: +34-958-160907
alm@iag.ugr.es
(J.A.)